Presynaptic plasma membrane Ca^{2+} ATPase isoform 2a regulates excitatory synaptic transmission in rat hippocampal CA3

Thomas P. Jensen[1], Adelaida G. Filoteo[2], Thomas Knopfel[3] and Ruth M. Empson[1,4]

[1]*School of Biological Sciences, Royal Holloway University of London, Egham, Surrey TW20 0EX, UK*
[2]*The Program in Molecular Neuroscience, Department of Biochemistry and Molecular Biology, Mayo Graduate School, Mayo Clinic, Rochester, MN 55905, USA*
[3]*Laboratory for Neuronal Circuit Dynamics, RIKEN Brain Science Institute, Wako-ishi, Saitama, 351-0198, Japan*
[4]*Department of Physiology, University of Otago School of Medical Sciences, Dunedin, New Zealand*

Plasma membrane calcium ATPase isoforms (PMCAs) are expressed in a wide variety of tissues where cell-specific expression provides ample opportunity for functional diversity amongst these transporters. The PMCAs use energy derived from ATP to extrude submicromolar concentrations of intracellular Ca^{2+} ($[Ca^{2+}]_i$) out of the cell. Their high affinity for Ca^{2+} and the speed with which they remove $[Ca^{2+}]_i$ depends upon splicing at their carboxy (C)-terminal site. Here we provide biochemical and functional evidence that a brain-specific, C-terminal truncated and therefore fast variant of PMCA2, PMCA2a, has a role at hippocampal CA3 synapses. PMCA2a was enriched in forebrain synaptosomes, and in hippocampal CA3 it colocalized with the presynaptic marker proteins synaptophysin and the vesicular glutamate transporter 1, but not with the postsynaptic density protein PSD-95. PMCA2a also did not colocalize with glutamic acid decarboxylase-65, a marker of GABA-ergic terminals, although it did localize to a small extent with parvalbumin-positive presumed inhibitory terminals. Pharmacological inhibition of PMCA increased the frequency but not the amplitude of mEPSCs with little effect on mIPSCs or paired-pulse depression of evoked IPSCs. However, inhibition of PMCA activity did enhance the amplitude and slowed the recovery of paired-pulse facilitation (PPF) of evoked EPSCs. These results indicated that fast PMCA2a-mediated clearance of $[Ca^{2+}]_i$ from presynaptic excitatory terminals regulated excitatory synaptic transmission within hippocampal CA3.

(Resubmitted 7 November 2006; accepted after revision 6 December 2006; first published online 14 December 2006)
Corresponding author R. M. Empson: Department of Physiology, University of Otago School of Medical Sciences, Dunedin, New Zealand. Email: ruth.empson@stonebow.otago.ac.nz

Plasma membrane Ca^{2+} ATPases (PMCAs), a family of P-type Ca^{2+} ATPases, are expressed in a variety of cell types where their main function is to extrude Ca^{2+} from the cytosol out of the cell. The PMCAs achieve this against the inward Ca^{2+} gradient, using energy derived from the hydrolysis of ATP (Carafoli, 1992). Moreover, their high affinity for Ca^{2+} ensures that they can remove intracellular Ca^{2+} ($[Ca^{2+}]_i$) even at submicromolar concentrations. For these reasons the PMCAs are considered to be a highly efficient and primary route for Ca^{2+} efflux during $[Ca^{2+}]_i$ transients within neurones (Thayer *et al.* 2002).

There are four PMCA isoforms, PMCA1–4. Each is the product of a different gene, and all are distributed in a cell-specific manner. PMCA2 and 3 are enriched within excitable cells such as muscle and neurones (Brandt *et al.* 1992; Zacharias & Kappen, 1999), where their faster extrusion rates, compared with the more ubiquitously expressed PMCA isoforms 1 and 4 (Brini *et al.* 2003), are ideally suited to control fast $[Ca^{2+}]_i$ transients.

Alternative splicing of the PMCA transcripts also provides a way to modify PMCA function and location, since splicing can give rise to PMCAs with distinct activation kinetics and localization (Caride *et al.* 2001*a*; Chicka & Strehler, 2003). In particular, splicing at the carboxy (C)-terminal splice site, the C site, produces two functionally distinct PMCA isoforms. The C-terminal truncated 'a' variant, compared with its full length 'b' variant, exhibits a decreased calmodulin dependence (Elwess *et al.* 1997) and a gain of PKC phosphorylation sites (Enyedi *et al.* 1997). PMCA 'a' splice variants are more rapidly activated by Ca^{2+}, and extrude $[Ca^{2+}]_i$ at a higher rate, leading to the idea that they are 'fast' PMCA variants (Caride *et al.* 2001*a*). In contrast, activation of

 DOI: 10.1113/jphysiol.2006.123901

the full length 'b' variant (Strehler & Zacharias, 2001) is delayed, compared with the 'a' variant, but once activated it maintains a high rate of Ca^{2+} extrusion long after $[Ca^{2+}]_i$ returns to basal levels (Caride *et al.* 2001*b*; Pottorf & Thayer, 2002). PMCA 'b' variants also contain a PDZ binding domain (PSD 95/Dlg/ZO-1) that allows PMCA2b to interact with selected postsynaptic proteins within dendritic spines (DeMarco & Strehler, 2001). This has led to the suggestion that the PMCA2b splice variant may be important for synapse function by controlling postsynaptic $[Ca^{2+}]_i$.

Rapid control of presynaptic $[Ca^{2+}]_i$ is also likely to be equally important for presynaptic function, given the importance of $[Ca^{2+}]_i$ for the control of transmitter release. In particular, rapid Ca^{2+} extrusion from the presynaptic terminal is expected, and the fast activation rate of PMCA 'a' splice variants makes them ideally suited to this task. Although PMCAs have been shown to exist at presynaptic sites (Fujii *et al.* 1996; Morgans *et al.* 1998; Juhaszova *et al.* 2000), where they provide one of the routes for presynaptic Ca^{2+} removal along with the Na^+/Ca^{2+} exchanger (Kim *et al.* 2005; Zenisek & Matthews, 2000; Usachev *et al.* 2002), there is no evidence for the functional consequence of this presynaptic location of PMCAs. Nor is there any indication as to which PMCA isoform or splice variant is critical.

In the present study we show that expression of the PMCA2 'a' splice variant is enriched within excitatory presynaptic terminals in the hippocampal CA3 region. We could not however, detect PMCA2a within GAD-65-positive inhibitory presynaptic terminals, although a subset of PV-positive terminals (presumed inhibitory) did express PMCA2a. Furthermore, pharmacological inhibition of PMCA activity revealed an enhancement of paired-pulse facilitation (PPF) and mEPSC frequency, while having little effect upon inhibitory synaptic transmission. Since both PPF and miniature synaptic transmission are regulated by presynaptic $[Ca^{2+}]_i$ (Zucker & Regehr, 2002; Emptage *et al.* 2001), and given the strong expression of PMCA2a at excitatory terminals, we propose a key role for PMCA2a during excitatory synaptic transmission in hippocampal CA3.

Methods

Hippocampal slice culture and slice preparation

Combined hippocampal-entorhinal cortex slice cultures were prepared as previously described (Jensen *et al.* 2004) from P7 (postnatal day 7) Wistar rats rapidly decapitated without anaesthesia to minimize unnecessary suffering. Slice cultures were maintained for 9–14 days *in vitro* before use in electrophysiology, immunohistochemistry or Western blotting. Acute hippocampal slices from young adult rats, following terminal anaesthesia (intraperitoneal pentobarbitone 140 mg kg^{-1}) that minimized unnecessary suffering were prepared as previously described (Jensen *et al.* 2004). All procedures were in accordance with the UK Animals (Scientific Procedures) Act 1986, and approved by the Royal Holloway Animal Welfare Committee.

SDS-PAGE and Western blotting

SDS-PAGE and Western blotting were carried out as previously described (Jensen *et al.* 2004). In brief, samples of equalized protein content (15 μg) were loaded onto 7.5% polyacrylamide gels, separated by electrophoresis and transferred to a nitrocellulose membrane using standard Western blotting techniques. Protein levels were controlled by *post hoc* analysis of Ponceau stains of transfers and Coomassie-stained gels to ensure equal protein loading.

Transferred proteins were probed using primary antibodies specific for N-terminal epitopes of total PMCA1, 2, 3 or 4 (NR1-3 and JA9, respectively, Abcam, Cambridge, UK) or antibodies specific for C-terminal epitopes PMCA1a–4a (Filoteo *et al.* 1997), and visualized on Kodak Biomax film using HRP-conjugated secondary antibodies (Dako Ltd, Glostrup, Denmark) with ECL substrates (Pierce, Illinois, USA).

Immunohistochemistry

Organotypic hippocampal slices were prepared for immunohistochemistry as previously described (Buckby *et al.* 2006) except for colocalization of PMCA2a with PSD-95 where a rapid fix (Castejón *et al.* 2004) was employed. Primary antibodies used were anti-PMCA1 (NR1 1 : 250), PMCA2 (NR2 1 : 250), PMCA1a (CR1a, 1 : 750) PMCA2a (CR2a, 1 : 750), PSD-95 (1 : 100, Cambridge Bioscience, Cambridge, UK), Synaptophysin (1 : 100 Santa Cruz Biotechnology, Santa Cruz, CA, USA) VGLUT1 (1 : 500, Synaptic Systems, Goettingen, Germany), GAD-65 and PV (1 : 100 and 1 : 250, respectively, Chemicon, Temecula, CA, USA). Secondary antibodies used were anti-rabbit Alexa 488 conjugates for single labelling, or anti-mouse Alexa 488 combined with an anti-rabbit Alexa 568 conjugate (all at 1 : 500; Invitrogen Ltd, Paisley, UK) for dual labelling and colocalization.

Confocal fluorescence microscopy and colocalization quantification

Using a modification of the method described by Buckby *et al.* (2006), we used a laser scanning confocal microscope (Radiance 2100, Carl Zeiss Ltd, Welwyn Garden City, UK) attached to an upright light microscope fitted with a 60× oil immersion objective (Eclipse model E600FN, Nikon, Tokyo, Japan) to image immunohistochemical labelling in the CA3 region of organotypic hippocampal slices. Fluorescence from Alexa 488 and 568 conjugates was obtained by excitation with the 488 nm line of an

Argon laser and the 543 nm line of a Green He/Ne laser, respectively. When both were used (simultaneously) for colocalization experiments, we employed lambda strobing and also collected the images separately to eliminate any possibility of bleed-through.

For colocalization experiments, we collected a total of 12, 62.23 μm × 62.23 μm fields of view in each slice (three in each of the CA3 statum oriens, pyramidal cell layer and stratum radiatum) as 512 × 512 pixel boxes. Using the colocalization function in Lasersharp (Carl Zeiss Ltd, Welwyn Garden City, UK), we determined Pearson's correlation values (a commonly used measure of colocalization) to analyse the extent of colocalization. All images were thresholded to include only the top 30% of pixel intensities from each image, and although this reduces Pearson's correlation values, it removes contributions from background fluorescence to the colocalization score. All quoted Pearson's correlation values refer to those determined in the pyramidal cell layer unless otherwise stated. Error values stated refer to the S.E.M., and significance was tested with unpaired *t* tests.

Electrophysiology

Organotypic hippocampal slices were transferred to a recording chamber on the stage of an upright light microscope (Eclipse model E600FN, Nikon, Tokyo, Japan) and superfused (2.5–3 ml min^{-1}) with artificial cerebrospinal fluid (aCSF, see below for composition) at 25°C. Whole-cell patch-clamp recordings were made using patch electrodes with tip resistances of 8–10 MΩ from visually identified CA3 pyramidal neurones held at −70 mV in voltage-clamp mode using an Axoclamp 2B (Axon Instruments, Union City, CA, USA) with a switching frequency of 40–50 kHz and a gain of 2–5 nA mV^{-1} with capacitance compensation adjusted. Pipette voltage was also continuously monitored to ensure that it decayed fully following current injection during the 30 : 70 duty cycle. In several cells, the clamp efficiency was estimated to be 80–90% by measurement of voltage deflections during subsequent EPSCs and EPSPs (measured in current clamp). Signals were amplified (×50) and filtered (dc/5 kHz) using a Neurolog amplifier (Digitimer Ltd, Welwyn Garden City, UK), then filtered further using a Humbug (Digitimer Ltd, Welwyn Garden City, UK). Only neurones with stable input resistances (measured during short 30 ms −5 mV square pulses) and requiring <0.2 nA holding current were accepted for recording. Input and series resistance were monitored regularly throughout the recordings, and varied <20%.

We evoked pairs of EPSCs at 0.033 Hz using minimal, local stimulation delivered via a monopolar stimulating electrode placed in stratum radiatum of CA3 that received 40 μs square pulses of 2–5 V using a constant voltage isolated stimulator (model DS2A-mkII, Digitimer Ltd, Welwyn Garden City, UK). Evoked EPSCs were insensitive to 5 μM DCG-IV, a group II mGluR agonist ((2*S*,2′*R*,3′*R*)-2-(2′,3′-dicarboxycyclopropyl)glycine), strongly supporting the absence of any mossy fibre component to the EPSCs, but were completely abolished by 100 μM AP5 (DL-2-amino-5-phosphonopentanoic acid) and 20 μM CNQX (6-cyano-7-nitroquinoxaline-2,3-dione), NMDA receptor and AMPA receptor antagonists, respectively. Pairs of monosynaptic IPSCs were evoked with local stimulation within the CA3 pyramidal layer (20–30 V) at a frequency of 0.05 Hz.

Data acquisition, stimulus triggering and analysis of evoked EPSCs and IPSCs was accomplished using Signal software (Cambridge Electronic Design Ltd, Cambridge, UK) on a PC connected to a 1401 plus (Cambridge Electronic Design Ltd, Cambridge, UK). Miniature (m)EPSCs/mIPSCs were recorded over 150 s epochs in control and treated conditions, data were then analysed off-line using Mini-Analysis software (Synaptosoft, Atlanta, GA, USA). mEPSCs/mIPSCs were detected if their amplitude was greater than the threshold of 5 pA, and were considered for analysis if their rise time was shorter than their decay time. To compare mEPSC populations between control and drug-treated conditions, median values of mEPSC inter-event-intervals (IEIs) and amplitudes were obtained under each condition for each cell and compared using paired *t* tests for statistical analysis. All error values stated in the text refer to S.E.M. The significance of shifts in cumulative probability curves of pooled mEPSC IEIs and amplitudes were also investigated using non-parametric two-sample Kolmogorov–Smirnov tests performed by Mini-Analysis (Synaptosoft, Atlanta, GA, USA). For both evoked and mEPSCs/IPSCs, further analysis of numerical data was accomplished with Excel (Microsoft, Redmond, WA, USA) and Prism 3.03 (Graphpad software, San Diego, CA, USA). In particular the $t_{1/2}$ values for the decay of evoked EPSC paired-pulse facilitation (PPF) and recovery of evoked IPSC paired-pulse depression (PPD) in individual cells were best determined using unconstrained single exponential fits using Prism 3.03; where for decay:

$$Y = A_1 e^{(-KX)} + \text{plateau}$$

where A_1 is the extrapolated PPF value at $X = 0$, where K is the rate constant, and where plateau is the minimum PPF reached, and for association:

$$Y = Y_{\max}\left(1 - e^{(-KX)}\right)$$

starting from zero, and where $Y_{\max}$ is the maximum value of PPD reached. Normalization of the PPF data used the extrapolated peak PPF value, A_1, obtained from the unconstrained exponential fits for each individual cell in order to normalize and therefore directly compare the

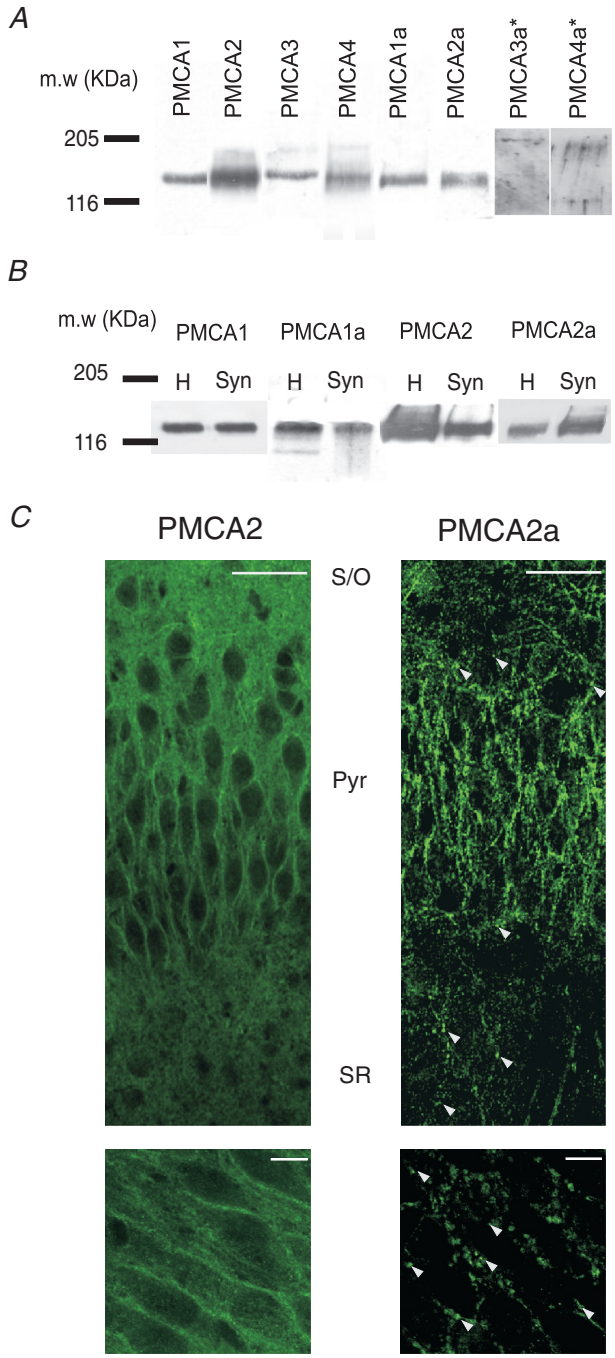

Figure 1. PMCA2a is selectively enriched in forebrain synaptosomes and shows a punctate distribution within hippocampal CA3

A, representative Western blots from hippocampal homogenates probed with antibodies raised against total PMCA isoforms 1–4 (lanes 1–4, left to right) or PMCA1a–4a (lanes 5–8 left to right). *B*, Western blots from forebrain homogenates (H) and synaptosomes (Syn) probed for total PMCA1, PMCA1a, total PMCA2 and PMCA2a. For all blots, 15 μg of protein from homogenate or synaptosome protein samples were loaded into their respective lane, 205 and 116 bars represent the approximate positions of these standard molecular weight markers. *C*, representative montages of the hippocampal CA3 region (top) or zoomed images of the CA3 pyramidal cell layer (bottom) labelled with antibodies raised against total PMCA2 (left panel) or PMCA2a (right panel); scale bars indicate a distance of 100 μm or 20 μm (top and bottom, respectively), and arrowheads indicate the location of PMCA2a punctae. S/O, Pyr and SR indicate the stratum oriens, pyramidal cell layer and stratum radiatum, respectively.

decay of PPF across all cells before and after carboxyeosin (CE) treatment.

Solutions

Artificial cerebrospinal fluid (aCSF) contained (mM) NaCl 126, KCl 2.5, NaH_2PO_4 1.2, $MgCl_2$ 1.3, $CaCl_2$ 2, $NaHCO_3$ 26, Glucose 10, and in experiments to record evoked EPSCs, 10 μM bicuculline methioidide (Sigma-Aldrich, Poole, UK), 5 μM CGP 52432 (Tocris Cookson, Bristol, UK) and 0.5 μM NBQX (1,2,3,4-tetrahydro-6-nitro-2,3-dioxo-benzo[f]quinoxaline-7-sulphonamide, Tocris Cookson, Bristol, UK) were included to reduce $GABA_A$ and $GABA_B$-ergic pre- and postsynaptic inhibition and polysynaptic activity, respectively. In experiments where evoked IPSCs were recorded, the extracellular solution contained 20 μM CNQX, 50 μM AP5, 5 μM CGP52432 and 5 μM naloxone hydrochloride. mEPSCs/IPSCs were recorded in the presence of 1 μM TTX (Tocris Cookson, Bristol, UK). For experiments using high pH, aCSF (pH 8.8) did not contain $NaHPO_4$, and NaCl concentration was altered to retain a constant Na^+ concentration as the pH was adjusted to 8.8 using NaOH. Carboxyeosin, CE (Invitrogen Ltd, Paisley, UK) and cyclopiazonic acid, CPA (Tocris Cookson, Bristol, UK) were stored as 1000× stock solutions in DMSO; all other drugs were stored as 1000× stocks in distilled H_2O. DMSO levels did not exceed 0.01%.

The intracellular solution for whole-cell recording of both EPSCs and IPSCs contained (mM) CsCl 120, NaCl 4, $MgCl_2$ 2.5, Hepes 10, EGTA 10, Na_2ATP 4, Na_2GTP 0.4, phosphocreatine 20 and QX314 5, pH was adjusted to pH 7.2 using CsOH and osmolarity to 305 mosmol l^{-1}.

Results

PMCA2a is enriched within synaptosome preparations

PMCAs are expressed within the hippocampus (Burette *et al.* 2003; Filoteo *et al.* 1997), and the hypothesis explored here is that Ca^{2+} extrusion at hippocampal synapses should preferentially use fast PMCA 'a' splice variants. We therefore began by using antibodies specific to PMCA 'a' splice variants (Filoteo *et al.* 1997) first in hippocampal tissue and then in forebrain synaptosomes as an initial screen to identify which, if any of the PMCA isoforms were present at synapses. Figure 1*A* shows strong immunoreactivity for all PMCA isoforms 1–4 in hippocampal tissue, using antibodies that recognize the N (amino)-terminus of these proteins and that do not

therefore discriminate between the shortened C-terminal 'a' *versus* the longer C-terminal 'b' splice variants, lanes 1–4. However, with antibodies targeted to the PMCA 'a' splice variant, C-terminal epitope, we could detect strong immunoreactivity at around the 130 KDa mark, with PMCA1a and 2a splice variant-specific antibodies. PMCA3a- and 4a-specific antibodies could not reveal any bands that were distinguishable from background noise at approximately 130 KDa, even during long exposure times and despite the fact that these antibodies did recognize PMCA3a and 4a within adult forebrain homogenates (data not shown).

This strong expression of PMCA1a and 2a splice variants in the hippocampus prompted us to investigate whether these two fast isoforms were also enriched at synapses. We therefore determined their expression within synaptosome preparations that contain both pre- and postsynaptic components. We noted a clear, relative enrichment of PMCA2a-specific immunoreactivity (Fig. 1*B*, far right) in synaptosomes compared with total PMCA2 (Fig. 1*B*, third panel). PMCA1 and PMCA1a were also present in the synaptosome fraction, but were not enriched (Fig. 1*B* first and second panels, respectively). Despite the presence of other PMCAs within the hippocampus, the results of this initial screen strongly suggested that PMCA2a was the predominant PMCA 'a' splice variant present at hippocampal synapses.

PMCA2a shows a punctate distribution within hippocampal CA3

Immunohistochemical studies of the hippocampal CA3 region revealed a pattern of discrete punctate PMCA2a labelling (arrowheads, Fig. 1*C*, right panel) in the pyramidal cell layer and throughout the dendritic layers, indicative of a synaptic distribution for PMCA2a. In contrast, labelling of total PMCA2 (Fig. 1*C*, left panel) showed a bright, uniform plasma membrane-like distribution throughout all layers of the hippocampus, with clearly outlined cell bodies in the pyramidal layer. Notably, labelling for PMCA1 and 1a (online Supplemental material, Supplementary Fig. 1) shared a distribution similar to total PMCA2, and further supported an isoform-specific pattern of PMCA2a expression in presumed synaptic puncta. The distinct punctate expression pattern of PMCA2a was also observed within CA3 of acutely prepared young adult rat and mouse hippocampal slices (Supplementary Fig. 2*A* and *B*), where we also verified the specificity of total PMCA2 and 2a labelling in hippocampal slices from PMCA2–/– knockout mice. No labelling above background was observed with either total PMCA2 or PMCA2a-specific antibodies (Supplementary Fig. 2*B*). In summary, the punctate distribution of the PMCA2a immunoreactivity within the hippocampal CA3 region, together with its enrichment within hippocampal synaptosomes, all pointed towards a synaptic location for PMCA2a. We next sought to further investigate this synaptic localization using immunohistochemical colocalization with known pre- and postsynaptic marker proteins.

PMCA2a is enriched at excitatory presynaptic terminals within hippocampal CA3

Figure 2*A* shows representative zoomed confocal images of the CA3 pyramidal cell layer from colocalization experiments where we compared PMCA2a (red) localization with synaptophysin (top, green), a predominantly presynaptic protein (Calakos & Scheller, 1994) and PSD-95 (bottom, green) a predominantly postsynaptic protein (Chetkovich *et al.* 2002). We frequently observed clear colocalization of PMCA2a within synaptophysin-containing punctae (Fig. 2*A*, merge, arrowheads) throughout all layers of the hippocampus (data not shown). In contrast, we rarely observed any colocalization between PMCA2a and PSD-95, with only a few bright punctae overlapping in all 36 of the images collected (Fig. 2*B*), yet we often observed close apposition of PMCA2a- and PSD-95- containing punctae (Fig. 2*B*, arrowheads). By using Pearson's correlation to quantify the level of colocalization between PMCA2a and synaptophysin across the different slice cultures, we determined a value of 0.22 ± 0.03, $n = 9$, that was significantly higher than the Pearson's correlation value of 0.04 ± 0.01 $n = 9$ observed for PMCA2a and PSD-95 ($P < 0.0001$, unpaired two-tailed students t test; Fig. 2*C*). Although PMCA1a was neither enriched within synaptosomes, nor demonstrated a punctate distribution, we further checked its colocalization with presynaptic marker proteins (Supplementary Fig. 3*A*) where we obtained mean Pearson's correlation values of <0.1, $n = 6$ (Supplementary Fig. 3*B*), indicating that PMCA1a was not present at presynaptic terminals. Together these results indicated that PMCA2a, and not PMCA1a, colocalized within presynaptic and not postsynaptic sites.

To further establish the nature of the synapses where PMCA2a was enriched, we investigated its localization in relation to an established marker of excitatory presynaptic terminals, the vesicular glutamate transporter 1 (VGLUT1) (Takamori *et al.* 2000). Colocalization of VGLUT1 (left, green, Fig. 3*A*) and PMCA2a (middle; red, Fig. 3*A*) was strong (Fig. 3*A*, merge lower panel; arrowheads), and in the pyramidal cell layer exhibited a mean Pearson's correlation value of 0.51 ± 0.01, $n = 9$. In the stratum radiatum (Fig. 3*B*), almost all VGLUT1-positive punctae colocalized with PMCA2a (Fig. 3*B*, merge lower panel; arrowheads), resulting in a mean Pearson's correlation value of 0.72 ± 0.03, $n = 9$, greater than seen in the pyramidal layer ($P < 0.0001$, unpaired two-tailed Student's t test). We also observed a similar pattern of expression and colocalization

in acutely prepared young adult rat hippocampal slices (data not shown). These combined results strongly supported the exclusive enrichment of the PMCA2a splice variant within excitatory glutamate-containing presynaptic terminals of hippocampal CA3.

Inhibition of PMCA activity enhances the frequency of mEPSCs in CA3 pyramidal neurones

The available evidence suggested a presynaptic location of PMCA2a at glutamatergic terminals and indicated a role for PMCA2a for the regulation of glutamate release. We therefore investigated the effect of reduced PMCA activity on isolated miniature excitatory postsynaptic currents (mEPSCs) in CA3 pyramidal cells using a specific inhibitor of PMCA activity (Gatto & Milanick, 1993) carboxyeosin (CE) at 10 μM.

We observed mEPSCs regularly in nine cells from nine slice cultures prepared from four animals. A 15 min treatment with 10 μM CE enhanced the frequency of mEPSCs (see Fig. 3*C*), seen also as a significant leftward shift in the cumulative histogram of pooled mEPSC inter-event intervals (IEIs) ($n = 9$ $P < 0.001$, Kolmogorov–Smirnov, two-sample test; Fig. 3*D*) and a decrease in the mean median inter-event interval from 635.0 ± 184.1 ms to 396.1 ± 117.1 ms ($n = 9$; $P < 0.01$ paired t test; see inset to Fig. 3*D*). Simultaneous with this increase in mEPSC frequency, 10 μM CE treatment did not affect either pooled mEPSC amplitude cumulative histograms ($n = 9$, $P = 0.15$, Kolmogorov–Smirnov two-sample test; Fig. 3*E*) or mean median mEPSC amplitudes ($n = 9$; $P = 0.99$ paired t test, see inset to Fig. 3*E*).

In order to further substantiate our findings following application of CE, we also investigated populations of mEPSCs in four further cells where we inhibited PMCA activity by an increase in extracellular pH from 7.4 to 8.8 (Willoughby *et al.* 2001; Wanaverbecq *et al.* 2003; Benham *et al.* 1992). In agreement with our results with 10 μM CE, these cells also showed a significant leftward shift in their cumulative histogram ($n = 4$, $P < 0.01$, Kolmogorov–Smirnov two-sample test) and the mean median IEI decreased from 675.5 ± 116.6 ms to 360.1 ± 47.6 ms ($n = 4$, $P < 0.05$ paired t test), both consistent with an enhanced frequency of mEPSCs when PMCA was inhibited. High extracellular pH, unlike the more specific PMCA inhibitor CE, also caused an increase in mEPSC amplitude, seen as a significant leftward shift in the cumulative histogram and an increase in the mean median mEPSC amplitude from 6.9 ± 0.9 pA to

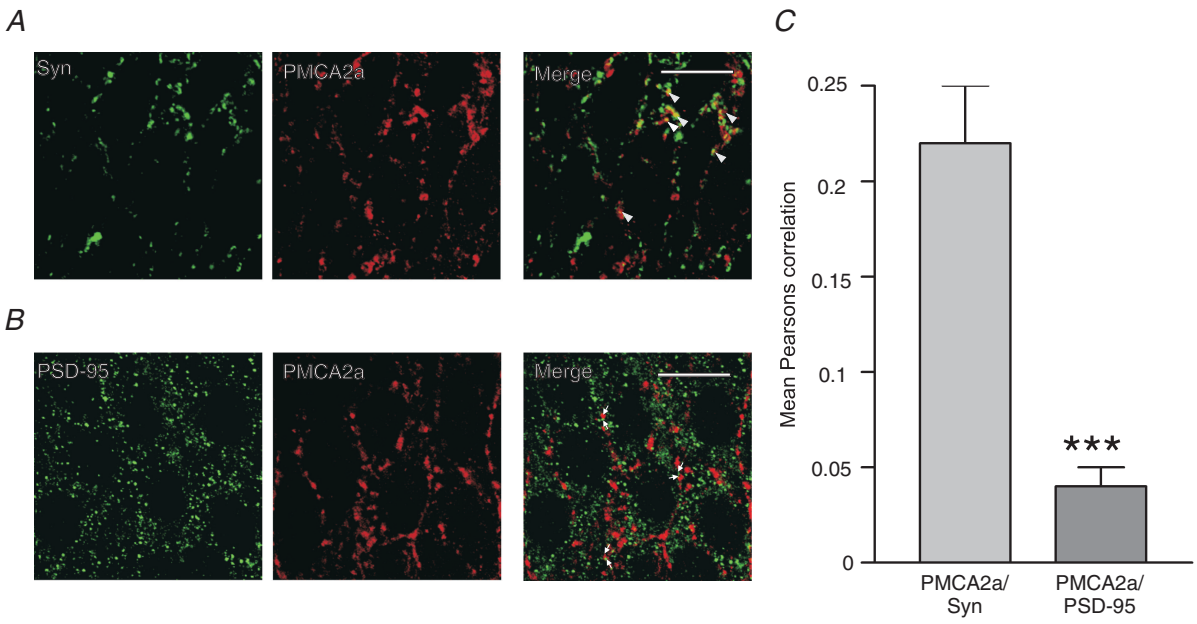

Figure 2. PMCA2a colocalizes with the presynaptic marker synaptophysin but not the postsynaptic marker PSD-95

A and *B*, representative confocal micrographs from the CA3 pyramidal cell layer showing typical colocalization of PMCA2a labelling (centre, red) with the presynaptic marker synaptophysin (Syn) and the postsynaptic marker PSD-95 (*B*) (left, green); merged images (*A* and *B*, right third panel) show colocalized pixels as yellow. Scale bars represent 20 μm, arrowheads indicate colocalized punctae in the third panel of *A* and arrows in the third panel of *B* indicate apposed PMCA2a and PSD-95 expression. *C*, quantification of colocalization using Pearson's correlation; the left bar shows mean Pearson's correlation values for PMCA2a and synaptophysin (Syn) and the right bar shows mean correlation values for PMCA2a and PSD-95. Values are means ± S.E.M. for $n = 9$, images from a minimum of nine images from four slice cultures prepared from four animals; ***$P < 0.0001$.

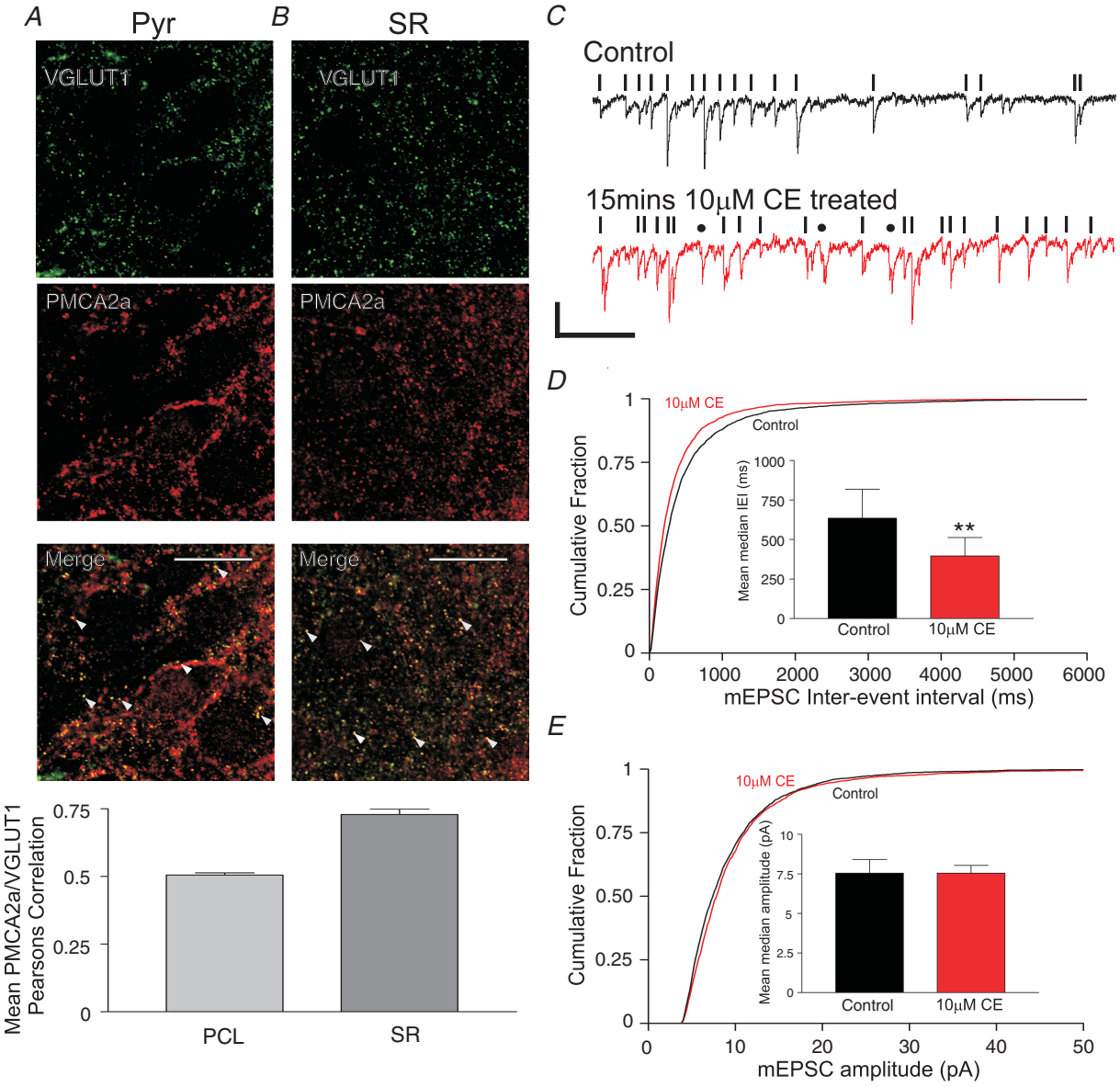

Figure 3. PMCA2a is present within VGLUT1-containing excitatory presynaptic terminals and inhibition of PMCA activity increases the frequency but not the amplitude of mEPSCs

A and *B*, representative confocal micrographs from the CA3 pyramidal cell layer (Pyr, *A*) and the CA3 stratum radiatum (SR, *B*) showing typical colocalization of PMCA2a labelling (centre, red) with the vesicular glutamate transporter 1 (VGLUT1; left, green); merged images (*A* and *B*, third panel right) show colocalized pixels as yellow. Scale bars represent 20 μm, arrowheads indicate colocalized punctae. *C*, quantification of colocalization using Pearson's correlation; the left bar shows mean Pearson's correlation values for PMCA2a and VGLUT1 in the pyramidal cell layer (Pyr) and the right bar shows mean correlation values for PMCA2a and VGLUT1 in the stratum radiatum (SR), values are means ± S.E.M. from a minimum of nine images from four slice cultures prepared from four animals; $^*P < 0.0001$. *C*, representative current traces recorded from a CA3 pyramidal cell held at −70 mV in the presence of 10 μM bicuculline and 1 μM TTX before (top, black line) and after 15 min of 10 μM CE treatment (bottom, red line); events accepted for analysis are highlighted by black vertical bars, events that were detected but did not fit criteria for analysis (see Methods) are indicated by a circle, scale bars represent 10 pA vertical and 1 s horizontal. *D*, a cumulative histogram of mEPSC inter-event intervals. The bar chart (inset) shows the mean median inter-event interval of mEPSCs in untreated cells (left, black) and after 10 μM CE treatment (right, red). *E*, cumulative histogram of mEPSC peak amplitudes (pA). The bar chart (inset) shows the mean median amplitude of mEPSCs in untreated cells (left, black) and after CE treatment (right, red). All error bars are ± S.E.M., $n = 9$ for control and CE-treated cells. $^*P < 0.01$ tested with paired, two-tailed *t* test.

8.28 ± 0.8 pA ($n = 4$; $P < 0.05$ paired t test), effects that may have arisen from the known non-specific effects of alkaline conditions on postsynaptic glutamate receptors (Taira *et al.* 1993) ($n = 4$, $P < 0.05$, Kolmogorov–Smirnov two-sample test; data not shown).

PMCA2a is present within some but not all inhibitory presynaptic terminals within hippocampal CA3

Although our results thus far clearly identified PMCA2a within excitatory presynaptic terminals of CA3, it was clear, especially within the pyramidal cell layer, that some PMCA2a punctae did not colocalize with excitatory presynaptic marker proteins. We therefore checked if PMCA2a colocalized with two known inhibitory presynaptic terminal marker proteins, GAD-65 (glutamic acid decarboxylase-65) (Gottlieb *et al.* 1986) and parvalbumin (PV) (Sloviter *et al.* 2003). As shown in Fig. 4*A* and *B*, both inhibitory presynaptic marker proteins showed a punctate expression pattern within the cell body layer of CA3, and the Pearson's correlations provided evidence for some colocalization of PV with PMCA2a but significantly less for GAD-65. The mean Pearson's correlation value for PMCA2a/GAD-65 was 0.087 ± 0.014 $n = 6$, significantly less than the mean Pearson's correlation value for PMCA2a/PV, at 0.29 ± 0.02 $n = 9$, $P < 0.0001$, unpaired two-tailed t test.

Inhibition of PMCA activity did not significantly alter the frequency of mIPSCs in CA3 pyramidal neurons

Consistent with our finding that PMCA2a did not colocalize extensively at inhibitory presynaptic terminals in CA3, we observed no significant alteration in the IEI or amplitude of mIPSCs (see Fig. 4*C* and *D*, where $P = 0.16$ in Kolmogorov–Smirnov for IEI, and where the mean median IEI was unchanged from 271 ± 37.4 ms in control to 228 ± 14 ms in CE-treated cells, $n = 9$, $P = 0.27$, paired t test) and in Fig. 4*C* and *E*, where $P = 0.5$ in Kolmogorov–Smirnov, mIPSC amplitude and mean median amplitude unchanged from 12.4 ± 0.9 pA to 11.7 ± 1.5 pA, $n = 9$, $P = 0.12$, paired t test).

Inhibition of PMCA activity also did not significantly alter the recovery of paired-pulse depression of evoked IPSCs in CA3 pyramidal neurons

We detected PMCA2a in a subset of PV-positive, presumably inhibitory presynaptic terminals within CA3. Given the importance of this slow Ca^{2+}-binding protein for the recovery of $[Ca^{2+}]_i$ within these inhibitory terminals for IPSC short-term plasticity (Collin *et al.* 2005; Jensen *et al.* 1999), we sought to determine if PMCA activity in these terminals contributed to GABA release probability, by investigating the paired-pulse depression of evoked IPSCs.

Consistent with the lack of effect of PMCA inhibition on mIPSCs, 10 μM CE had little effect upon the paired-pulse ratio of evoked IPSCs in CA3, see Fig. 5*A*, black *versus* red symbols and traces, over all interstimulus intervals ($P > 0.05$, two-way ANOVA). Furthermore, the rate of the recovery from PPD that is dependent on presynaptic residual $[Ca^{2+}]_i$ in inhibitory terminals (Zucker & Regehr, 2002; Jensen *et al.* 1999) was also unaffected by loss of PMCA activity. This recovery was best fitted with a single exponential association, and as shown in Fig. 5*B*, the means of individual recovery rates for cells before and after treatment with 10 μM CE were not different (mean values were 39.1 ± 6.1 ms under control conditions compared with 42.4 ± 5.6 ms in the presence of 10 μM CE, $P = 0.71$, t test, $n = 6$).

Inhibition of PMCA activity enhanced paired-pulse facilitation (PPF) of evoked EPSCs in CA3 pyramidal neurons

Previous studies have indicated that the time course of PPF is directly related to the recovery of the presynaptic $[Ca^{2+}]_i$ transient (Wu & Saggau, 1994; Regehr *et al.* 1994). We therefore proposed that if enriched PMCA2a within the presynaptic terminals of CA3 neurones was important for Ca^{2+} clearance from this compartment, then PPF should be influenced by inhibition of PMCA activity. For this reason we investigated the effect of PMCA inhibition on the amplitude and time course of PPF, as an indirect indicator of the rate of the recovery of the presynaptic residual $[Ca^{2+}]_i$ transient.

We recorded from 24 CA3 pyramidal neurones from separate slice cultures prepared from six animals. Robust PPF (Fig. 6*A*) of evoked EPSCs occurred in these cells following paired stimulation with a 50 ms interstimulus interval (ISI) when the resulting mean paired-pulse ratio (calculated as the peak amplitude of EPSC2/EPSC1) was 2.1 ± 0.1, $n = 6$. In 16 neurones, application of 10 μM CE clearly and reversibly enhanced PPF as shown for a single cell in Fig. 6*A*. This alteration occurred in the absence of any significant change in the amplitude of the first EPSC or the input resistance of the cell, see Fig. 6*B*, all from the same cell (mean values remained unchanged from 52.0 ± 9.6 pA and 275.9 ± 19.9 MΩ, $n = 9$ after 10 μM CE treatment, $P = 0.75$ and 0.92, respectively, paired t test). Rise times and decay times of the evoked EPSCs also remained unchanged before and after 10 μM CE treatment ($P > 0.48$ for both, paired t tests). This result provided good evidence that inhibition of PMCA by 10 μM CE under our experimental conditions did not affect the post-synaptic response, and may be attributed to the high concentration of the Ca^{2+} chelator EGTA (10 mM) present in the intracellular patch solution that thoroughly buffered

postsynaptic $[Ca^{2+}]_i$. We were also alert to the possibility that our results could have arisen if CE inhibited P-type Ca^{2+} ATPases of the endoplasmic reticulum (SERCAs) and so indirectly raised intraterminal $[Ca^{2+}]_i$. Given the rather low concentration of CE used (10 μM) this is unlikely (Gatto & Milanick, 1993), but we further confirmed in three cells treated with the SERCA inhibitor cyclopiazonic acid (30 μM, CPA) that PPF was unchanged

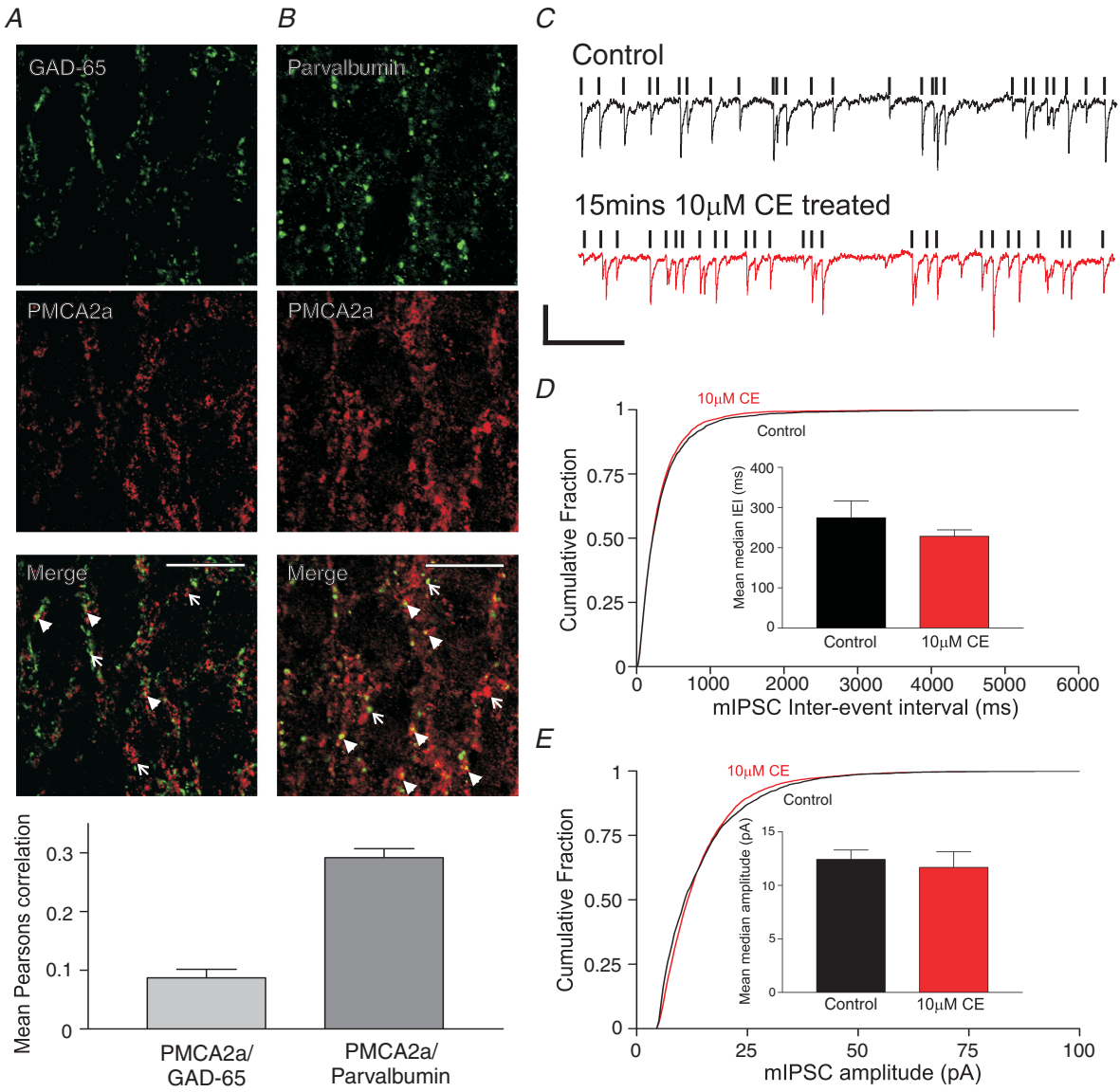

Figure 4. PMCA2a is present within a subset of PV-containing inhibitory presynaptic terminals but inhibition of PMCA activity does not significantly influence the frequency or amplitude of mIPSCs
A and *B*, representative confocal micrographs from the CA3 pyramidal cell layer of GAD-65 (*A*) and PV (*B*), green, upper panels, colocalized with PMCA2a (red); merged images (*A* and *B*, third panel) show colocalized pixels as yellow and some are identified with arrowheads, whereas arrows indicate PMCA2a punctae that are not colocalized. Scale bars represent 20 μm. Below the confocal micrographs the bar graph shows quantification of colocalization using Pearson's correlation; the left bar shows mean Pearson's correlation values for PMCA2a and GAD-65, and the right bar shows mean correlation values for PMCA2a and PV, values are means ± S.E.M. from a minimum of six slices. *C*), representative current traces of mIPSCs recorded from a CA3 pyramidal cell held at −70 mV in the presence of TTX before (top, black line) and after 15 min of 10 μM CE treatment (bottom, red line); events accepted for analysis are highlighted by black vertical bars (see Methods), scale bars represent 15 pA vertical and 1 s horizontal. *D*, cumulative histogram of mIPSC inter-event intervals. The bar chart (inset) shows the mean median inter-event interval of mIPSCs in untreated cells (left, black) and after 10 μM CE treatment (right, red). *E*, cumulative histogram of mIPSCs peak amplitudes (pA). The bar chart (inset) shows the mean median amplitude of mIPSCs in untreated cells (left, black) and after CE treatment (right, red). All error bars are ± S.E.M., $n = 9$ for control and CE-treated cells.

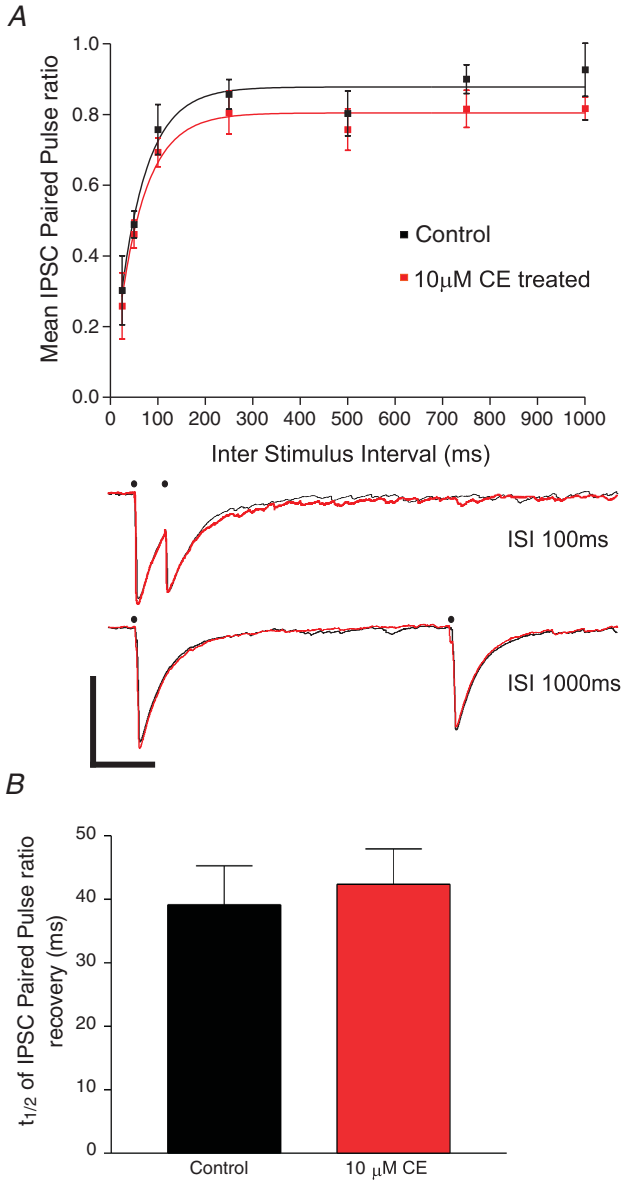

Figure 5. Inhibition of PMCA activity does not alter the amplitude or the kinetics of recovery of paired-pulse depression of evoked IPSCs

A, the mean paired-pulse ratio (IPSC2/IPSC1) of stimulus-evoked IPSCs from CA3 pyramidal neurones plotted against the interstimulus interval (ISI, ms), filled black squares indicate mean paired-pulse ratios from control cells, while filled red squares indicate the mean paired-pulse ratios from cells treated with 10 μM CE for 15 min, error bars are ± S.E.M., $n = 6$ for control and 10 μM CE-treated cells at all time points. Lower panel, representative current traces recorded from the same CA3 pyramidal cell held at −70 mV before (black lines) and after 15 min of 10 μM CE treatment (red lines). IPSCs were evoked with interstimulus intervals of 100 ms (top) and 1000 ms (bottom) at the time points highlighted by filled dots. Note the lack of any effect of CE on PPD at both short and long ISI, but note also the small (approx 5–10 pA) increase in the amplitude of the first evoked IPSC that was seen in 3/6 cells. Scale bars represent 150 pA vertical and 200 ms horizontal. *B*, mean half-time for recovery of the paired-pulse depression of evoked IPSCs determined from single exponential fits of the recovery of paired-pulse depression in individual cells before (filled black bar) and after (filled red bar) 10 μM CE.

before and after CPA ($P = 0.56$ paired t test, data not shown).

As expected, when the interstimulus interval between the paired stimulations was increased, the mean PPF

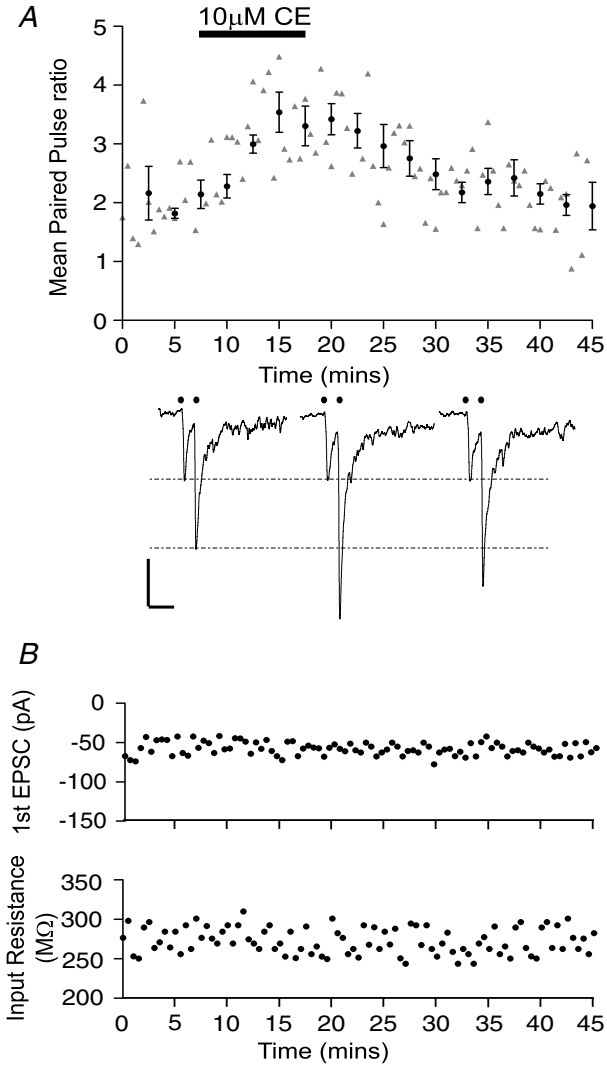

Figure 6. Inhibition of PMCA activity increases paired-pulse facilitation of evoked EPSCs, by enhancing the second EPSC, in a reversible and specific manner

A, application of 10 μM CE (represented by the horizontal black bar) increases the paired-pulse ratio recorded every 30 s, grey triangles for individual data points. Filled circles and error bars represent a running average ± S.E.M. over 2.5 min intervals. Below the graph are representative current traces recorded from the same CA3 pyramidal cell held at −70 mV, where small filled black circles represent the time of delivery of the stimulus, before application of CE (left) during CE application (middle) and 15 min after removal of CE (right), dashed black lines represent amplitudes of the first EPSC (black) and the control second EPSC following 10 μM CE treatment. In three neurones, 10 μM CE application increased the 50 ms paired-pulse ratio from 2.0 ± 0.1 to 3.1 ± 0.2 ($n = 3$; $P < 0.05$; paired t test) that was partially reversed 15 min after the removal of CE back to 2.4 ± 0.1 ($n = 3$; $P = 0.07$ paired t test). All scale bars represent 50 pA vertical and 100 ms horizontal. *B*, in the same cell shown in *A* the amplitude of the first EPSC (top) and cell input resistance (lower) recorded every 30 s during treatment with CE (shown by the horizontal black bar in *A*).

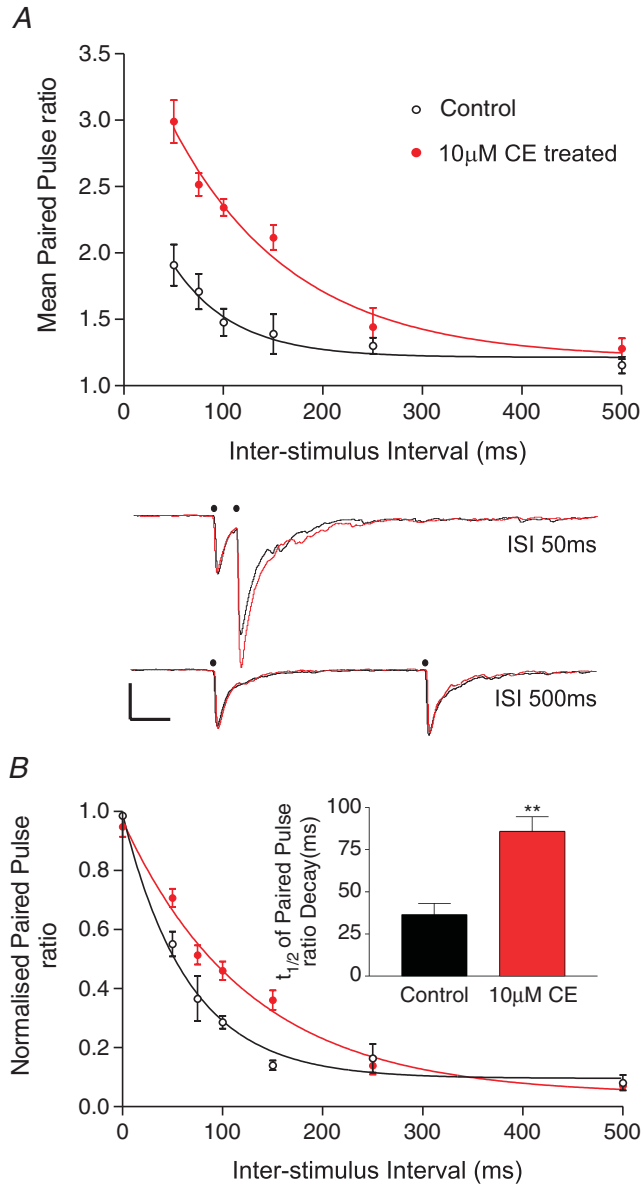

Figure 7. Inhibition of PMCA activity slows the recovery of paired-pulse facilitation of evoked EPSCs in CA3 pyramidal neurones
A, the mean paired-pulse ratio (EPSC2/EPSC1) of stimulus-evoked EPSCs from CA3 pyramidal neurones plotted against the interstimulus interval (ISI, ms), open circles indicate mean paired-pulse ratios from control cells, while filled red circles indicate the mean paired-pulse ratios from cells treated with 10 μM CE for 15 min, error bars are $\pm$ S.E.M., $n > 5$ for control and 10 μM CE-treated cells at all time points. Curves, black, control and red, CE, represent an unconstrained single exponential fit to this mean data. Lower panel, representative current traces recorded from the same CA3 pyramidal cell held at -70 mV before (black lines) and after 15 min of 10 μM CE treatment (red lines). EPSCs were evoked with ISIs of 50 ms (top) and 500 ms (bottom) at the time points highlighted by small filled black circles. Note the lack of any major influence of CE at the longer ISI. All scale bars represent 50 pA vertical and 100 ms horizontal. *B*, the normalized recovery of PPF in six cells before (open black circles) and after 10 μM CE (closed red circles), where the recovery of the PPF was fitted in each individual cell with a single exponential and then normalized using the extrapolated maximum paired-pulse ratio obtained from the A1 value as described in Methods. The inset bar graph shows the mean half-time for PPF decay for individual cells based upon individual single exponential fits before and after 10 μM CE, black and red bars, respectively. $^{**}P < 0.01$ tested with paired, two-tailed *t* test.

returned towards control levels, see Fig. 7*A*, black lines. This recovery occurred with a mean half-time of 42.4 ms as calculated from a single exponential decay of the mean PPF values, and presumably reflected the recovery of residual $[Ca^{2+}]_i$ in the presynaptic terminals. Treatment with 10 μM CE (Fig. 7*A*, red symbols and lines) significantly enhanced PPF ($P < 0.0001$, two-way ANOVA) at all inter-stimulus intervals except 250 ms and 500 ms, and increased the mean half-time of the single exponential recovery of the mean PPF to 84.5 ms. This slowed recovery of PPF in the presence of CE was more easily seen when the individual single exponential fits for the recovery of the PPF in five control and five CE-treated cells were normalized according to their extrapolated peak PPF, as shown in Fig. 7*B*. A direct comparison of the half-time of recovery of the PPF for these individual cells showed a clear prolongation of the recovery of PPF in CE-treated cells, see inset to Fig. 7*B*. The mean values of the PPF recovery changed from 36.4 ± 6.7 ms before, compared with 85.8 ± 8.6 ms after CE ($n = 6$, $P < 0.01$, *t* test) values not dissimilar to the exponential recoveries estimated from the mean, non-normalized values in Fig. 7*A*.

These results were all consistent with a delay in the removal of $[Ca^{2+}]_i$ from presynaptic terminals within CA3 following inhibition of the fast PMCA2a by CE. In doing so, short-term synaptic plasticity was enhanced during the period when the PMCA was critically required for fast clearance of $[Ca^{2+}]_i$ from the restricted cytosolic volume of the terminal.

Our combined analysis of evoked and mEPSC and IPSC behaviour within CA3 neurones when PMCA activity was reduced, together with our biochemical and immunohistochemical localization of PMCA2a, confirmed a functional role for the specific enrichment of PMCA2a within excitatory presynaptic terminals in CA3.

Discussion

The present study aimed to identify the location and function of isoforms of the Ca^{2+} extrusion protein, the PMCA, at synapses within hippocampal CA3.

PMCA2a, a fast PMCA isoform, is enriched at excitatory presynaptic terminals in hippocampal CA3

As expected, all PMCA isoforms were expressed within the hippocampus (Burette *et al.* 2003; Jensen *et al.* 2004; Filoteo *et al.* 1997). To expand upon this earlier work,

we developed the hypothesis that rapid extrusion of Ca^{2+} from synapses by fast PMCA 'a' splice variants was critical for synapse function. We therefore focused our initial search to identify fast PMCA isoforms within synapses, by using PMCA 'a' splice variant-specific antibodies to screen a synapse-enriched biochemical preparation, synaptosomes. The result identified an exclusive enrichment of PMCA2a within synaptosomes (Fig. 1*B*, far right panel). Furthermore, immunohistochemistry within hippocampal CA3 revealed PMCA2a immunoreactivity as discrete punctae consistent with a synaptic distribution (Fig. 1*C*, right panel), whereas total PMCA2 immunoreactivity appeared throughout the plasma membrane of pyramidal neurones (Fig. 1*C*, left panel).

With this supporting evidence for a synaptic location for PMCA2a, we chose to analyse its location further by colocalizing with known synaptic proteins. Our initial results identified a clear colocalization between PMCA2a and the presynaptic marker synaptophysin (Fig. 2*A*), but not with the postsynaptic density protein PSD-95 (Fig. 2*B* and *C*). Furthermore, PMCA2a exhibited strongest colocalization with VGLUT1, a marker of excitatory presynaptic terminals (Takamori *et al.* 2000) throughout all layers of hippocampal CA3 (Fig. 3A and *B*), but with greatest prominence in stratum radiatum (Fig. 3*B*) where the majority of VGLUT1-positive terminals exist. However, some PMCA2a-positive punctae in the pyramidal cell layer did not colocalize with VGLUT1, and raised the possibility that PMCA2a might also be present at inhibitory synaptic terminals. Subsequent colocalization of PMCA2a with two markers of inhibitory presynaptic terminals, GAD-65 and PV, revealed that only a subset of PMCA2a punctae were at PV-positive presumed presynaptic inhibitory terminals (see Fig. 4*A* and *B*). Our combined results therefore supported the enrichment of PMCA2a at excitatory presynaptic terminals, with the proviso that some also existed at PV-containing inhibitory terminals, although we also cannot ignore the possibility that PMCA2a may be expressed in other types of CA3 terminals, such as those containing peptides.

PMCA activity is important for excitatory synaptic transmission and the time course of short-term plasticity in hippocampal CA3

Armed with clear evidence for an enrichment of PMCA2a at excitatory presynaptic terminals, we next sought to identify whether the location of this fast PMCA isoform was functional. Although a number of studies have identified the ability of PMCAs to regulate presynaptic $[Ca^{2+}]_i$ (Zenisek & Matthews, 2000; Kim *et al.* 2005), none have so far related this function to the regulation of synaptic transmission or to the presence, or even the enrichment, of a specific PMCA isoform. We began by investigating whether spontaneous miniature synaptic transmission, at both excitatory (mEPSCs) and inhibitory (mIPSCs) synapses, was altered following application of the PMCA inhibitor, carboxyeosin, CE. Consistent with the more prominent location of PMCA2a at excitatory terminals, CE readily enhanced the frequency of mEPSCs without altering their amplitude. The most likely explanation for this result following presynaptic inhibition of PMCA2a was an increase in the probability of glutamate release following elevation of resting cytosolic $[Ca^{2+}]_i$ within the presynaptic terminal (as previously reported in ventricular myocytes when PMCA was inhibited; Choi & Eisner, 1999). The increase in mEPSC frequency may also have arisen if raised basal cytosolic $[Ca^{2+}]_i$ enhanced Ca^{2+}-induced Ca^{2+} release (CICR), especially in CA3 presynaptic terminals where spontaneous CICR-mediated Ca^{2+} transients underlie around half of the mEPSCs (Emptage *et al.* 2001), and where even a small rise in basal $[Ca^{2+}]_i$ could amplify the probability of CICR-mediated glutamate release.

In contrast to the ability of CE to alter mEPSCs, inhibition of PMCA activity had no significant effect on mIPSCs and was consistent with the lack of colocalization of PMCA2a with GAD-65 and the lower level of colocalization of PMCA2a with PV (at least compared with VGLUT1). A viable explanation for our physiological result is that PV-positive terminals make up only about 30% of the total number of inhibitory synapses (Ribak *et al.* 1990) and since only a subset of these contained PMCA2a, our inability to detect any significant changes in a large population of mIPSCs following CE may not be surprising. A similar explanation may underlie our inability to detect any significant change in the recovery of paired-pulse depression of evoked IPSCs, even though previous studies show that alterations in slow Ca^{2+} buffering within cerebellar and hippocampal inhibitory presynaptic terminals do alter the time course and extent of IPSC depression (Collin *et al.* 2005; Jensen *et al.* 1999). At present we cannot exclude a role for PMCA2a during synaptic transmission at this subset of PV-containing inhibitory terminals, but it may become important for example during rapid, repetitive firing of the interneurones or during asynchronous release.

However, both our immunocytochemistry and the physiological effects of CE on mEPSCs provided strong supporting evidence for a functional role for PMCA2a at excitatory presynaptic terminals. It was therefore important to test if the absence of PMCA activity could alter the kinetics of presynaptic $[Ca^{2+}]_i$ clearance from these excitatory terminals. As the most accessible indicator of presynaptic $[Ca^{2+}]_i$ we chose to investigate paired-pulse facilitation (PPF) of excitatory synaptic transmission. In hippocampal synapses the recovery time course of PPF coincides with the time course of recovery of the

residual presynaptic $[Ca^{2+}]_i$ transient (Wu & Saggau, 1994; Regehr *et al.* 1994). Therefore, if the fast PMCA2a splice variant was important for controlling presynaptic $[Ca^{2+}]_i$ transients by extrusion, we would expect inhibition of the PMCA at this site to prolong the time for presynaptic $[Ca^{2+}]_i$ to recover and in doing so to enhance both the magnitude and time course of PPF. As shown in Fig. 6*A*, selective inhibition of the PMCA with 10 μM CE resulted in a reversible enhancement of PPF without any significant effect upon either the first EPSC or the input resistance or membrane potential of the neurones. This result indicated that PMCA-mediated Ca^{2+} efflux from the terminals, presumably via the fast PMCA2a splice variant, was important for the regulation of their residual $[Ca^{2+}]_i$, particularly during the first 250 ms following the first rise in terminal $[Ca^{2+}]_i$ (see Fig. 7*A* and *B*). This was significant since modelling of cytosolic $[Ca^{2+}]_i$ in the parallel fibre to Purkinje neurone synapse suggests that PMCA-mediated Ca^{2+} clearance occurs during the early phase after the initial $[Ca^{2+}]_i$ rise in the parallel fibre terminal, when the high-capacity Na^+/Ca^{2+} exchanger is likely to be in reverse mode (Regehr, 1997). In contrast, elegant measurements of presynaptic $[Ca^{2+}]_i$ in the calyx of Held show that inhibition of PMCA prolongs the slower phase of the Ca^{2+} recovery following a single action potential (Kim *et al.* 2005). Therefore the relative timing and contributions of the PMCA and the Na^+/Ca^{2+} exchanger to Ca^{2+} extrusion at CA3 presynaptic terminals remain important questions.

Although our proposal that PMCA inhibition enhanced PPF through slowed recovery of residual presynaptic $[Ca^{2+}]_i$ was attractive, we were alert to other mechanisms by which reduced PMCA activity could enhance residual $[Ca^{2+}]_i$ and PPF. In salamander cone photoreceptors, PMCA inhibition indirectly enhances CICR (Krizaj *et al.* 2003) via enhancement of cytosolic $[Ca^{2+}]_i$ levels. Since CICR provides some of the source for residual Ca^{2+} that underlies PPF at CA3 synapses (Emptage *et al.* 2001), this could be relevant to our findings. However, PPF was unchanged when intracellular Ca^{2+} stores were depleted, suggesting that the main source of residual $[Ca^{2+}]_i$ underlying PPF in this study was from the opening of voltage-gated calcium channels (Carter *et al.* 2002). A CICR-based mechanism to explain the enhanced PPF when PMCA was inhibited seems unlikely.

To summarize, a variety of approaches supports our hypothesis that clearance of $[Ca^{2+}]_i$ by the fast 'a' splice variant of PMCA2a from within CA3 hippocampal presynaptic terminals is functionally significant for excitatory synaptic transmission and glutamate release.

How and why does PMCA2a exist within hippocampal presynaptic terminals?

Given the enrichment of PMCA2a at CA3 presynaptic terminals, it is interesting to speculate how this may occur. One possible explanation resides in a consensus sequence for golgi localization present at the PMCA2a C-terminus that is consistent with targeting of PMCA2a to the secretory pathway (Strehler & Zacharias, 2001). Moreover, a number of additional lines of evidence support the idea that PMCA2a may reside within synaptic vesicles. In addition to our results here, PMCAs also colocalize with vesicular markers SV-2 and synaptotagmin I (Fujii *et al.* 1996; Juhaszova *et al.* 2000), while ultrastructural and, more recently, proteomic analyses have identified PMCA within synaptic vesicles (Fujii *et al.* 1996; Blondeau *et al.* 2004), although in all these studies the isoform is not clear. It is tempting to speculate that a vesicular location of PMCA2a could ensure a tight coupling between transmitter release and local Ca^{2+} efflux while also providing an efficient mechanism to traffic PMCA2a within the presynaptic terminal.

It is important also to consider the wider implications of the presence of a fast-acting Ca^{2+} efflux system at hippocampal presynaptic terminals. Known alterations in expression of PMCAs during hippocampal development (Jensen *et al.* 2004) and ageing (Janicki *et al.* 1996), as well as after pathological insults such as ischaemia (Lehotsky *et al.* 2002) and status epilepticus (Ketelaars *et al.* 2004) could profoundly influence the maintenance and plasticity of hippocampal synaptic transmission.

References

Benham CD, Evans ML & McBain CJ (1992). Ca^{2+} efflux mechanisms following depolarisation evoked calcium transients in cultured rat sensory neurones. *J Physiol* **455**, 567–583.

Blondeau F, Ritter B, Allaire PD, Wasiak S, Girard M, Hussain NK, Angers A, Legendre-Guillemin V, Roy L, Boismenu D, Kearney RE, Bell AW, Bergeron JJ & McPherson PS (2004). Tandem MS analysis of brain clathrin-coated vesicles reveals their critical involvement in synaptic vesicle recycling. *Proc Natl Acad Sci U S A* **101**, 3833–3838.

Brandt P, Neve RL, Kammesheidt A, Rhoads RE & Vanaman TC (1992). Analysis of the tissue-specific distribution of mRNAs encoding the plasma membrane calcium-pumping ATPases and characterization of an alternately spliced form of PMCA4 at the cDNA and genomic levels. *J Biol Chem* **267**, 4376–4385.

Brini M, Coletto L, Pierobon N, Kraev N, Guerini D & Carafoli E (2003). A comparative functional analysis of plasma membrane Ca^{2+} pump isoforms in intact cells. *J Biol Chem* **278**, 24500–24508.

Buckby LE, Jensen TP, Smith PJ & Empson RM (2006). Network stability through homeostatic scaling of excitatory and inhibitory synapses following inactivity in CA3 of rat organotypic hippocampal slice cultures. *Mol Cell Neurosci* **31**, 805–816.

Burette A, Rockwood JM, Strehler EE & Weinberg RJ (2003). Isoform-specific distribution of plasma membrane Ca^{2+} ATPase in the rat brain. *J Comp Neurol* **467**, 464–476.

Calakos N & Scheller RH (1994). Vesicle-associated membrane protein and synaptophysin are associated on the synaptic vesicle. *J Biol Chem* **269**, 24534–24537.

Carafoli E (1992). The Ca^{2+} pump of the plasma membrane. *J Biol Chem* **267**, 2115–2118.

Caride AJ, Filoteo AG, Penheiter AR, Paszty K, Enyedi A & Penniston JT (2001*a*). Delayed activation of the plasma membrane calcium pump by a sudden increase in Ca^{2+}: fast pumps reside in fast cells. *Cell Calcium* **30**, 49–57.

Caride AJ, Penheiter AR, Filoteo AG, Bajzer Z, Enyedi A & Penniston JT (2001*b*). The plasma membrane calcium pump displays memory of past calcium spikes. Differences between isoforms 2b and 4b. *J Biol Chem* **276**, 39797–39804.

Carter AG, Vogt KE, Foster KA & Regehr WG (2002). Assessing the role of calcium-induced calcium release in short-term presynaptic plasticity at excitatory central synapses. *J Neurosci* **22**, 21–28.

Castejón OJ, Fuller L & Dailey ME (2004). Localization of synapsin-I and PSD-95 in developing postnatal rat cerebellar cortex. *Dev Brain Res* **151** (1–2), 25–32.

Chetkovich DM, Bunn RC, Kuo SH, Kawasaki Y, Kohwi M & Bredt DS (2002). Postsynaptic targeting of alternative postsynaptic density-95 isoforms by distinct mechanisms. *J Neurosci* **22**, 6415–6425.

Chicka MC & Strehler EE (2003). Alternative splicing of the first intracellular loop of plasma membrane Ca^{2+}-ATPase isoform 2 alters its membrane targeting. *J Biol Chem* **278**, 18464–18470.

Choi HS & Eisner DA (1999). The role of sarcolemmal Ca^{2+}-ATPase in the regulation of resting calcium concentration in rat ventricular myocytes. *J Physiol* **515**, 109–118.

Collin T, Chat M, Lucas MG, Moreno H, Racay P, Schwaller B, Marty A & Llano I (2005). Developmental changes in parvalbumin regulate presynaptic Ca^{2+} signaling. *J Neurosci* **25** (1), 96–107.

DeMarco SJ & Strehler EE (2001). Plasma membrane Ca^{2+}-ATPase isoforms 2b and 4b interact promiscuously and selectively with members of the membrane- associated guanylate kinase family of PDZ (PSD95/Dlg/ZO-1) domain-containing proteins. *J Biol Chem* **276**, 21594–21600.

Elwess NL, Filoteo AG, Enyedi A & Penniston JT (1997). Plasma membrane Ca^{2+} pump isoforms 2a and 2b are unusually responsive to calmodulin and Ca^{2+}. *J Biol Chem* **272**, 17981–17986.

Emptage NJ, Reid CA & Fine A (2001). Calcium stores in hippocampal synaptic boutons mediate short-term plasticity, store-operated Ca^{2+} entry, and spontaneous transmitter release. *Neuron* **29**, 197–208.

Enyedi A, Elwess NL, Filoteo AG, Verma AK, Paszty K & Penniston JT (1997). Protein kinase C phosphorylates the 'a' forms of plasma membrane Ca^{2+} pump isoforms 2 and 3 and prevents binding of calmodulin. *J Biol Chem* **272**, 27525–27528.

Filoteo AG, Elwess NL, Enyedi A, Caride A, Aung HH & Penniston JT (1997). Plasma membrane Ca^{2+} pump in rat brain. Patterns of alternative splices seen by isoform-specific antibodies. *J Biol Chem* **272**, 23741–23747.

Fujii JT, Su FT, Woodbury DJ, Kurpakus M, Hu XJ & Pourcho R (1996). Plasma membrane calcium ATPase in synaptic terminals of chick Edinger–Westphal neurons. *Brain Res* **734**, 193–202.

Gatto C & Milanick MA (1993). Inhibition of the red blood cell calcium pump by eosin and other fluorescein analogues. *Am J Physiol Cell Physiol* **264**, C1577–C1586.

Gottlieb DI, Chang YC & Schwob JE (1986). Monoclonal antibodies to glutamic acid decarboxylase. *Proc Natl Acad Sci U S A* **83**, 8808–8812.

Janicki PK, Horn JL, Singh G, Franks WT, Janson VE & Franks JJ (1996). Increased anesthetic requirements for isoflurane, halothane, enflurane and desflurane in obese Zucker rats are associated with insulin-induced stimulation of plasma membrane Ca^{2+}-ATPase. *Life Sci* **59**, L269–L275.

Jensen K, Lambert JD & Jensen MS (1999). Activity-dependent depression of GABAergic IPSCs in cultured hippocampal neurons. *J Neurophysiol* **82**, 42–49.

Jensen TP, Buckby LE & Empson RM (2004). Expression of plasma membrane Ca^{2+} ATPase family members and associated synaptic proteins in acute and cultured organotypic hippocampal slices from rat. *Dev Brain Res* **152**, 129–136.

Juhaszova M, Church P, Blaustein MP & Stanley EF (2000). Location of calcium transporters at presynaptic terminals. *Eur J Neurosci* **12**, 839–846.

Ketelaars SO, Gorter JA, Aronica E & Wadman WJ (2004). Calcium extrusion protein expression in the hippocampal formation of chronic epileptic rats after kainate-induced status epilepticus. *Epilepsia* **45**, 1189–1201.

Kim M-H, Korogod N, Schneggenburger R, Ho W-K & Lee S-H (2005). Interplay between Na^+/Ca^{2+} exchangers and mitochondria in Ca^{2+} clearance at the calyx of Held. *J Neurosci* **25**, 6057–6065.

Krizaj D, Lai FA & Copenhagen DR (2003). Ryanodine stores and calcium regulation in the inner segments of salamander rods and cones. *J Physiol* **547**, 761–774.

Lehotsky J, Kaplan P, Murin R & Raeymaekers L (2002). The role of plasma membrane Ca^{2+} pumps (PMCAs) in pathologies of mammalian cells. *Front Biosci* **7**, d53–d84.

Morgans CW, El Far O, Berntson A, Wassle H & Taylor WR (1998). Calcium extrusion from mammalian photoreceptor terminals. *J Neurosci* **18**, 2467–2474.

Pottorf WJ & Thayer SA (2002). Transient rise in intracellular calcium produces a long-lasting increase in plasma membrane calcium pump activity in rat sensory neurons. *J Neurochem* **83**, 1002–1008.

Regehr WG (1997). Interplay between sodium and calcium dynamics in granule cell presynaptic terminals. *Biophys J* **73**, 2476–2488.

Regehr WG, Delaney KR & Tank DW (1994). The role of presynaptic calcium in short-term enhancement at the hippocampal mossy fiber synapse. *J Neurosci* **14**, 523–537.

Ribak CE, Nitsch R & Seress L (1990). Proportion of parvalbumin-positive basket cells in the GABAergic innervation of pyramidal and granule cells of the rat hippocampal formation. *J Comp Neurol* **300**, 449–461.

Sloviter RS, Zappone CA, Harvey BD, Bumanglag AV, Bender RA & Frotscher M (2003). 'Dormant basket cell' hypothesis revisited: relative vulnerabilities of dentate gyrus mossy cells and inhibitory interneurons after hippocampal status epilepticus in the rat. *J Comp Neurol* **459**, 44–76.

Strehler EE & Zacharias DA (2001). Role of alternative splicing in generating isoform diversity among plasma membrane calcium pumps. *Physiol Rev* **81**, 21–50.

Taira T, Smirnov S, Voipio J & Kaila K (1993). Intrinsic proton modulation of excitatory transmission in rat hippocampal slices. *Neuroreport* **4**, 93–96.

Takamori S, Rhee JS, Rosenmund C & Jahn R (2000). Identification of a vesicular glutamate transporter that defines the glutamatergic phenotype in neurons. *Nature* **407**, 189–194.

Thayer SA, Usachev YM & Pottorf WJ (2002). Modulating Ca^{2+} clearance from neurons. *Front Biosci* **7**, d1255–1279.

Usachev YM, DeMarco SJ, Campbell C, Strehler EE & Thayer SA (2002). Bradykinin and ATP accelerate Ca^{2+} efflux from rat sensory neurons via protein kinase C and the plasma membrane Ca^{2+} pump isoform 4. *Neuron* **33**, 113–122.

Wanaverbecq N, Marsh SJ, Al Qatari M & Brown DA (2003). The plasma membrane calcium-ATPase as a major mechanism for intracellular calcium regulation in neurones from the rat superior cervical ganglion. *J Physiol* **550**, 83–101.

Willoughby D, Thomas R & Schwiening C (2001). The effects of intracellular pH changes on resting cytosolic calcium in voltage-clamped snail neurones. *J Physiol* **530**, 405–416.

Wu LG & Saggau P (1994). Presynaptic calcium is increased during normal synaptic transmission and paired-pulse facilitation, but not in long-term potentiation in area CA1 of hippocampus. *J Neurosci* **14**, 645–654.

Zacharias DA & Kappen C (1999). Developmental expression of the four plasma membrane calcium ATPase (Pmca) genes in the mouse. *Biochim Biophys Acta* **1428**, 397–405.

Zenisek D & Matthews G (2000). The role of mitochondria in presynaptic calcium handling at a ribbon synapse. *Neuron* **25**, 229–237.

Zucker RS & Regehr WG (2002). Short-term synaptic plasticity. *Annu Rev Physiol* **64**, 355–405.

Acknowledgements

We thank Professor Emanuel Strehler and Dr Stella Elkabes for generous donation of PMCA 'a' splice variant specific antibodies and prefixed PMCA2–/– brain tissue, respectively, and Dr Molly Garside for synaptosome preparations and comments on the manuscript. This work was funded by the Epilepsy Research Foundation, UK and BBSRC Grant BBS/B/05338.

Supplemental material

The online version of this paper can be accessed at:
DOI: 10.1113/jphysiol.2006.123901
http://jp.physoc.org/cgi/content/full/jphysiol.2006.123901/DC1
and contains supplemental material consisting of three figures.

Figure S1. Expression of PMCA1 and 1a within the CA3 pyramidal cell layer of hippocampal slice cultures

Figure S2. PMCA2a expression is punctate throughout the CA3 pyramidal cell layer of acute hippocampal slices and also specific to PMCA2

Figure S3. PMCA1a expression is not detectable at excitatory presynaptic terminals in hippocampal CA3

This material can also be found as part of the full-text HTML version available from http://www.blackwell-synergy.com